Park et al. Applied Biological Chemistry (2022) 65:75
https://doi.org/10.1186/s13765-022-00744-4

KSABC
The Korean Society for Applied Biological Chemistry

ARTICLE

Open Access

Removal of phosphates using eggshells and calcined eggshells in high phosphate solutions

Jong-Hwan Park[1†], Ah-Young Choi[2†], Su-Lim Lee[2], Jae-Hoon Lee[2], Jun-Suk Rho[2], Seong-Heon Kim[3] and Dong-Cheol Seo[2*]

Abstract

This study was conducted to evaluate the phosphate sorption properties of eggshell (ES) and calcined ESs (C-ESs) in a high-concentration phosphate solution. The C-ESs yield decreased rapidly at 900 °C, indicating that the $CaCO_3$ constituting the ES was converted to CaO by the high calcination temperature. The optimum calcination temperature for phosphate removal using C-ES was 900 °C. The actual sorption amount of phosphate by ES and C-ES900 was in agreement with the Langmuir isothermal sorption equation, and the maximum sorption capacities derived from this equation were 178.6 and 270.3 mg/g, respectively. The sorption rate of phosphate by ES and C-ES900 was divided into two stages: an initial fast sorption stage, followed by a slow sorption stage. The sorption of phosphate by ES was dominantly influenced by the initial pH and salt concentration, whereas C-ES900 exhibited a constant sorption capacity regardless of environmental changes. The SEM–EDS and XRD results demonstrated that phosphate was successfully adsorbed on the ES and C-SE900 surfaces. In this study, it was found that the sorption of phosphate by ES occurred via ion exchange and precipitation reactions and that the sorption of phosphate by C-ES900 was dominantly affected by precipitation. Above all, C-ES can be applied as an effective adsorbent for removing high concentrations of phosphate under a wide range of environmental conditions.

Keywords: Calcination, Eggshell, Phosphate, Sorption, Wastewater

Introduction

Phosphorus (P) is sporadically discharged from various sources, such as domestic sewage, agricultural land, and urban areas, and easily flows into the water system via rainfall [1]. In particular, excessive phosphate in rivers and lakes is known to promote phytoplankton growth and cause eutrophication [2, 3]. Eutrophication reduces the dissolved oxygen concentration in water, which is devastating to aquatic life and can ultimately reduce aquatic biodiversity [4]. In addition, various toxic substances produced by eutrophication accumulate in the food chain, ultimately endangering human health. In general, eutrophication occurs when the phosphate concentration is above 0.02 mg/L in rivers and lakes [5]. Therefore, the government closely regulates the concentration of phosphate in the water system. The removal and recovery of phosphorus from aquatic ecosystems or discharged from various nonpoint sources is critical to maintain a healthy environment.

The ion exchange resin method, biological denitrification, chemical reduction, reverse osmosis method, electrodialysis method, and chemical precipitation method are common techniques to remove phosphorus from wastewater [6, 7]. However, these treatment methods not only have high installation and operation costs but also have difficulty maintaining a stable phosphorus

†Jong-Hwan Park and Ah-Young Choi are contributed equally to this work

*Correspondence: drseodc@gmail.com

[2] Division of Applied Life Science (BK21) and Institute of Agriculture and Life Science, Gyeongsang National University, Jinju 52828, South Korea
Full list of author information is available at the end of the article

treatment efficiency [8]. In addition, most mechanical methods generate a substantial amount of sludge, which can also be regarded as waste and cause secondary pollution. Over the past few decades, adsorption has become a promising and economical phosphorus treatment technology to overcome these problems [9, 10].

Recently, mineral- and waste-based and synthetic adsorbents have been developed for phosphorus adsorption [11–13]. However, mineral-based and synthetic adsorbents are limited in treating wastewater with high concentrations of phosphorus generated on a large scale because of their high cost and low treatment efficiency. In addition, low-cost and high-efficiency adsorbents based on waste such as fly ash and sludge may be effective for phosphorus removal, but they are unsuitable for large-scale facilities because of the risk of leaching toxic substances [14]. In this regard, the development of a new adsorbent for phosphorus treatment that is economically feasible, efficient, and stable is of great interest. In particular, several studies have reported that the stably developed calcium-rich material with adsorbed phosphate can be utilized as a fertilizer and industrial material [15–17]. Therefore, if calcium-rich waste can be used as a resource and produced as an adsorbent that can remove phosphate, it is expected to be a technology that can simultaneously satisfy waste reduction, wastewater treatment and development of new materials.

Recently, the demand for eggs in South Korea has been approximately 650,000 t/yr. As the demand for eggs gradually increases annually, the production of eggshells (ESs) is also expected to increase to approximately 70,000 t/yr, which is 11% of the weight of eggs, most of which are landfilled without special recycling. Therefore, using ESs as a phosphorus adsorbent could compensate for the problems of existing adsorbents while reducing waste. The main component of ES is calcium carbonate ($CaCO_3$), which has been studied extensively as a material capable of effectively adsorbing/precipitating phosphate via ion exchange and complex formation in aqueous solutions [18]. In particular, it has been reported that calcined ESs (C-ESs) prepared at high calcination temperatures have a higher affinity for phosphate than pure ESs owing to the physicochemical changes from the treatment [19, 20]. However, most of the studies on the sorption properties of conventional ESs and C-ESs were performed at low phosphate concentrations, indicating that their sorption capacity may have been underestimated. In addition, there have been no reports on the behavioral characteristics of phosphates in ESs and C-ESs when high concentrations of phosphates are introduced under various environmental changes. Therefore, the purpose of this study was to determine the maximum sorption capacity of phosphate by ESs and C-ESs in a high-concentration phosphate solution and to evaluate their sorption characteristics under various environmental conditions.

Materials and methods

Preparation and characteristics of ESs and C-ESs

The ESs used in this experiment were collected from a local restaurant and washed with distilled water to remove foreign substances from the surface before calcination. The washed ESs were dried in a dry oven (JS Research INC, Korea) at 60 °C and then pulverized, sealed, and stored to prevent contamination with air before use. C-ESs were prepared by calcining a crucible with crushed ESs and adjusting the calcination temperature to 300–900 °C in a calcination furnace (Nabertherm, Germany). The temperature of C-ESs in the calcination furnace was maintained for 1 h (residence time) after reaching the target temperature, and then it was set to cool naturally. In this experiment, the C-ESs are denoted as C-ESx, where x is the calcination temperature. The yield of the prepared C-ESs was calculated using the weight difference between the raw material and C-ES after calcination. The pH and carbon and inorganic contents of the ESs and C-ESs were determined using a pH meter (Mettler Toledo, Swiss), elemental analyzer (Thermo Fisher Scientific, USA), and Inductively Coupled Plasma-Optical Emission Spectrometry (ICP-OES, PerkinElmer, USA). The changes in the surface functional groups of the C-ESs owing to the calcination temperature were analyzed using Fourier Transform Infrared Spectroscopy (FTIR, PerkinElmer, USA).

Phosphate-sorption characteristics of ESs and C-ESs

The phosphate-sorption characteristics of the ESs and C-ESs were analyzed by varying the calcination temperature, initial phosphate concentration, reaction time, initial pH, adsorbent dose, coexisting anions, and salt concentration. Briefly, 25 mL of a 100 mg/L phosphate solution (pH 5) was injected into a polyethylene tube containing 0.05 g of ESs and C-ESs prepared at different pyrolysis temperatures. The polyethylene tube containing the sample and phosphate solution was stirred on a stirrer for 24 h and then filtered through No. 6 filter paper (Toyo Roshi Kaisha, Ltd, Japan). The concentration of phosphate in the filtrate was determined using the molybdenum blue-ascorbic acid method. The amount of phosphate adsorbed per gram of ES and C-ES was calculated considering the initial and final phosphate concentrations. To determine the effects of the initial phosphate concentration on the phosphate-sorption characteristics of the ES and C-ES900, the initial phosphate concentration was adjusted from 2.5 mg/L to 1000 mg/L. Subsequent experimental procedures and analyses were

performed in the same manner as previously described. The sorption results of ES and C-ES900 according to the initial phosphate solution were applied to the Freundlich and Langmuir isothermal sorption models, and the equations, plats, and constants related to the two models are presented in Additional file 1: Table S1.

Additionally, the effects of environmental changes, such as reaction time (0.25–24 h), initial pH (2–10), adsorbent dose (0.1–1.0 g), coexisting ions (Cl^-, NO_3^-, SO_4^{2-} and HCO_3^-), and salt concentration (0–3% of NaCl) were analyzed using an initial phosphate concentration of 1000 mg/L. All this experiment was performed in triplicate, and the results are presented as mean and standard deviation in the figures.

Phosphate-sorption mechanisms of ESs and C-ESs

The concentration of Ca^{2+} released from ES and C-ES900 in the presence or absence of phosphate was evaluated with distilled water and a phosphate solution of 1000 mg/L adjusted to pH 5, and the concentration of released Ca^{2+} ions was measured using ICP-OES. The surface properties, elemental distribution, and crystalline structure of ES and C-ES900 before and after phosphate sorption were determined using *Scanning Electron Microscopy* (*SEM*) with Energy-Dispersive X-ray Spectroscopy (SEM–EDS, Jeol, Japan) and *X-ray diffraction* (XRD, Bruker, USA).

Results and discussions

Characteristics of ESs and C-ESs according to the calcination temperature

Table 1 lists the characteristics of the ESs and C-ESs according to the thermal decomposition temperature. At pyrolysis temperatures from 300 to 800 °C, the yield of C-ES was in the range of 90.31–96.2%, and although it slightly decreased with the increase in pyrolysis temperature, the difference was not significant. In contrast, the yield of C-ES900 was 65.1%, which was significantly lower than that of C-ES800. In general, pure ES is mostly composed of $CaCO_3$, which remains relatively stable up to a calcination temperature of 800 °C. However, the $CaCO_3$ in ESs is converted to CaO at a calcination temperature of 900 °C [21], with a substantial amount of CO_2 generated during the conversion. Therefore, the yield of ES900 was drastically reduced compared with that of pure ES. The carbon content of ES was 18.6% whereas that of C-ES900 was 6.9%, indicating that the carbon in the ES was emitted as CO_2 during the calcination process ($CaCO_3$ $CaO + CO_2$). Our results are consistent with those of Park et al. [22] and Choi et al. [23], who reported that the carbon content in oyster and crawfish shells composed of $CaCO_3$ also decreased depending on the calcination temperature. While the specific surface area of ES was 0.87 m^2/g, it tended to increase as the calcination temperature increased from 300 °C to 700 °C. However, from the calcination temperature of 800 °C or higher, the specific surface area tended to decrease rapidly. These results suggest that $CaCO_3$-based ES at high temperatures over 800 °C contributed to recrystallization into CaO and/or $Ca(OH)_2$ during the calcination process.

The pH of the ESs was 7.99, and although C-ESs were thermally decomposed at 300–800 ℃, their pH was in the range of 7.58–8.35, and there was no significant difference in the pH of the C-ESs. However, the pH of ESs calcined at 900 °C was 11.47, which was higher than that of the conventional ESs and ESs calcined (C-ESs) at 300–800 °C. This is because $CaCO_3$ was converted to CaO at 900 ℃, and the dissolution of CaO in the aqueous phase ($CaO + H_2O$ Ca^{2+} $+2OH^-$) caused the high alkalinity. In addition, $CaCO_3$ in ES is partially converted to $Ca(OH)_2$ during the calcination process, which also causes high alkalinity in the aqueous. The carbon content in the ESs was 30.7%, which tended to increase slightly with increasing the calcination temperature. This is because the Ca content per unit weight of C-ES increased as moisture, impurities, and CO_2 in the ES were lost

Table 1 Properties of ES and C-ESs

	Yield (%)	S_{BET} (m^2/g)	pH (5:1)	C %	K	Na	Ca	Mg	P
ES	–	0.87	7.99	18.55	0.05	0.05	30.74	0.27	0.08
C-ES300	96.2	1.26	7.97	17.56	0.06	0.05	39.65	0.26	0.08
C-ES400	95.7	3.69	7.85	17.07	0.07	0.07	37.95	0.25	0.08
C-ES500	94.5	6.48	7.76	16.64	0.07	0.07	36.39	0.26	0.08
C-ES600	93.4	16.25	7.58	15.88	0.02	0.03	35.48	0.25	0.08
C-ES700	92.6	21.14	7.70	15.58	0.06	0.07	38.60	0.26	0.08
C-ES800	90.1	14.21	8.35	14.96	0.06	0.06	40.46	0.35	0.11
C-ES900	65.1	8.24	11.47	6.90	0.02	0.03	41.60	0.28	0.09

during the calcination. The contents of K, Na, Mg, and P of the C-ESs did not vary significantly with the calcination temperature.

The functional groups of the ESs and C-ESs prepared at different pyrolysis temperatures are shown in Fig. 1. The peak generated at a wavelength of 562 cm^{-1} in C-ES900 is attributed to Ca–O [24]. The peaks assigned to the wavelengths of 712, 872, and 1,423 cm^{-1} indicated that symmetric and asymmetric C–O stretching, respectively, contributed to CO_3^{2-} [25, 26], and these peaks were observed in both ESs and C-ESs. Although the $CaCO_3$ in the ES was converted to CaO during the high-temperature calcination process, these peaks were observed because some $CaCO_3$ remained in the C-ES900. The little peaks found at wavelengths 1798 and 2513 cm^{-1} in ES and C-ES could be attributed to $CaCO_3$ [27]. A peak related to -OH was observed at a wavelength of 3642 cm^{-1} in C-ES800 and C-ES900, which is closely related to $Ca(OH)_2$. In addition, these peaks tended to increase depending on the thermal decomposition temperature. These results demonstrate that $CaCO_3$ based ES is converted to CaO and/or $Ca(OH)_2$ during the calcination process.

The above results confirmed that both ESs and C-ESs were mostly composed of C and Ca, but their crystalline structures are different. In a phosphate solution, substantial amounts of Ca^{2+} ions on the surface of the ESs will elute and react with phosphate ions to form a compound and adsorb onto the surface. Although the chemical compositions of ECs and C-ESs may be similar, their maximum phosphate-sorption capacity and characteristics vary due to their different crystalline structures. Therefore, future research should focus on the phosphate-sorption characteristics of ESs and C-ESs under various sorption environmental conditions.

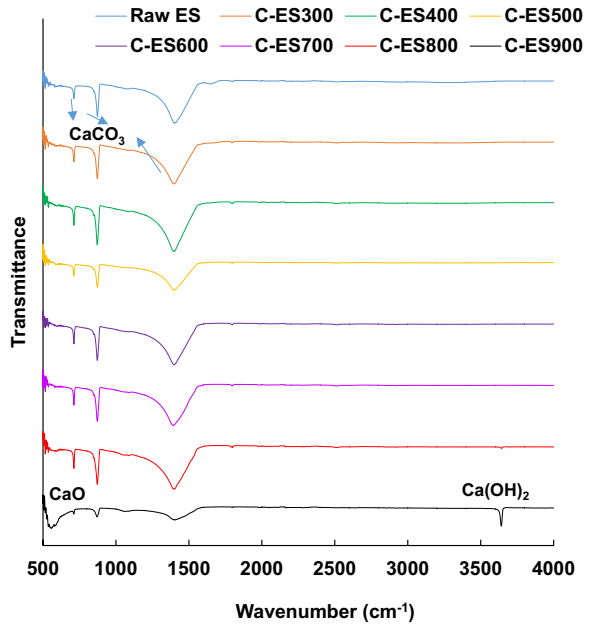

Fig. 1 Changes of functional group in ES and C-ESs derived from different calcination temperature

Phosphate-sorption characteristics of ESs and C-ESs

Calcination temperature

Additional file 1: Fig. S1 shows the phosphate-sorption characteristics of C-ESs according to the pyrolysis temperature. In the initial 100 mg/L phosphate solution (pH 5), the amount of phosphate adsorbed by pure ESs was 30.9 mg/g and that of C-ESs prepared at calcination temperatures of 300–600 °C did not vary significantly from that of pure ESs. However, the phosphate-sorption capacity of C-ES700 was reduced by 30% compared with that of pure ESs. Panagiotou et al. [28] and Lee et al. [20] also reported that the phosphate-sorption capacity of C-ESs prepared at 700 °C was lower than that of C-ESs prepared at other pyrolysis temperatures. This is because the $CaCO_3$ in the ESs was converted into another crystalline form that is poorly soluble in an aqueous solution before the conversion to CaO. The amounts of phosphate adsorbed using C-ES800 and C-ES900 were 40.3 and 56.3 mg/g, respectively, which were higher than that using pure ESs. Köse and Kıvanç [21] reported that the optimum calcination temperature for removing phosphate using C-ESs is 800 °C, which may be owing to the different initial phosphate concentrations used in the experiment. In particular, C-ES900 has a higher phosphate sorption capacity than C-ES prepared at other calcination temperatures, because most of its composition is in the form of CaO, which is easily dissolved in water to form Ca–P precipitates. According to a report by Lee et al. [20], during the calcination process, the specific surface area of the ESs increases owing to the emission of CO_2, and the surface exhibits a positive charge, which is further improved as the pyrolysis temperature increases. These factors also contribute to the high sorption of phosphate when using C-ES900. In this study, the optimum temperature for phosphate sorption with C-ESs was 900 °C. Therefore, the sorption characteristics of phosphate under various environmental conditions were investigated by focusing on pure ESs and C-ES900.

Initial phosphate concentration

Figure 2 shows the phosphate-sorption characteristics of ES and C-ES900 according to the initial phosphate concentration. The amount of phosphate adsorbed by ESs tended to increase as the concentration of the initial phosphate increased, and it was confirmed that equilibrium was reached in an initial phosphate

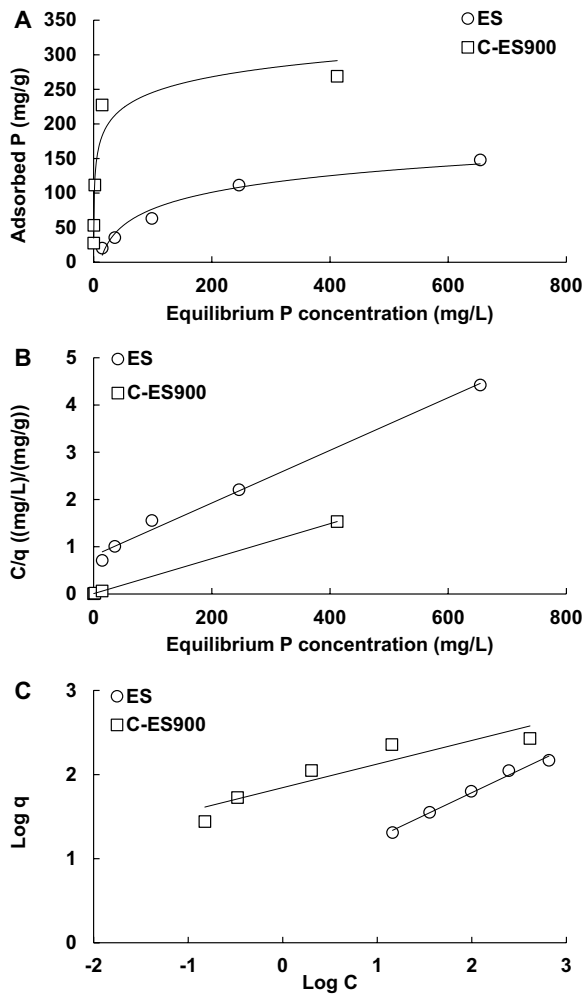

Fig. 2 Adsorption isotherm of phosphate by ES and C-ES900 [**A** Amount of phosphate adsorbed by EC and C-ES900, **B** Freundlich isotherm model, and **C** Langmuir isotherm model]

solution of approximately 1000 mg/L. These results confirmed that the reaction between the phosphate and Ca^{2+} ions eluted from the ES was predominantly affected by the phosphate concentration. However, when using C-ES900, the phosphate was almost completely adsorbed up to an initial phosphate concentration of 2.5–500 mg/L, but the amount adsorbed was limited when the initial phosphate concentration was 1000 mg/L. Because the amount of Ca^{2+} ions eluted from the CaO-based C-ES900 was reduced, the sorption was limited with the high concentration of phosphate. An isothermal sorption model equation was applied to evaluate the phosphate sorption mechanisms of ES and C-ES900 based on the initial phosphate concentration. The actual amount of phosphate adsorbed by ES and C-ES900 was in agreement with the Langmuir isothermal adsorption equation, and the maximum sorption capacities derived from this equation were 178.6 and 270.3 mg/g, respectively (Table 2). In general, Langmuir isothermal adsorption means that contaminants are bound by a chemical reaction as a monomolecular layer on the surface of an adsorbent with uniform binding energy, which is different from the Freundlich isothermal adsorption (physically adsorbed by a complex multi-molecular layer). According to literature survey, the amount of phosphate adsorbed by ESs and C-ESs was reported to vary from 0.4 to 44.25 mg/g [19, 21, 29, 30], which was lower than that presented in the current study. The difference in the sorption amounts reported in this study and previous studies may be due to the conditions used in the experiment. As can be seen from our results, the amount of phosphate adsorbed by ES is dominantly affected by the initial phosphate concentration. However, the phosphate concentrations used in the previous study ranged from 1 to 200 mg/g, which are much lower than those used in the current study. The initial pH is also an important factor in the sorption of phosphate by ESs. In most of the underestimated results, the pH of the phosphate solution was adjusted to 7; however, the initial pH used in this study was adjusted to 5. At the initial pH of 7, the amount of Ca^{2+} ions eluted from the ESs was relatively low, limiting the reaction with the phosphate ions to form Ca–P.

Table 2 The parameter estimates and coefficients of determination (R^2) for fit of the isotherm equation to experimental data of phosphate adsorption at ES and C-ES900

	Freundlich adsorption isotherm			Langmuir adsorption isotherm		
	K	1/n	R^2	a	b	R^2
ES	5.2	0.5342	0.9868	178.6	0.007	0.9917
C-ES900	69.9	0.2803	0.8553	270.3	0.487	1.0000

K: adsorption capacity of phosphate

1/n: an empirical parameter related to the intensity of sorption

a: maximum adsorption capacities of phosphate (mg/g)

b: binding strength constant of phosphate

Contact time

The results of phosphate sorption using ES and C-ES900 according to the reaction time are shown in Fig. 3A. The amount of phosphate adsorbed by ESs tended to increase continuously until 8 h after the start of the reaction, after which the sorption amount remained relatively constant. However, the amount of phosphate adsorbed by C-ES900 started to increase rapidly when the reaction began and almost reached equilibrium after 4 h. In conclusion, the phosphate sorption rates of ES and C-ES900 were divided into two stages. The first step was an increase in the sorption amount depending on the reaction time, and the second step was maintaining a constant sorption amount regardless of the reaction time after reaching equilibrium. The amount of contaminants adsorbed by the adsorbent in the initial stage of the reaction continuously increased, because most of the binding sites capable of adsorbing contaminants in the adsorbent were empty. However, when the binding sites of these adsorbents were saturated over time, the sorption amount no longer increased. In particular, the initial fast sorption of phosphate by the Ca-based adsorbents is influenced by the surface precipitation of the dissolved Ca^{2+} ions from the adsorbent surface rather than by adsorption. In our results, both the calcium-based ES and C-ES900 are considered to be dominated by precipitation during the phosphate-sorption process. In particular, the phosphate-sorption rate of C-ES900 was higher than that of ES, because the CaO constituting the C-ES900 dissolves more easily in an aqueous solution containing phosphate than the $CaCO_3$ constituting ES.

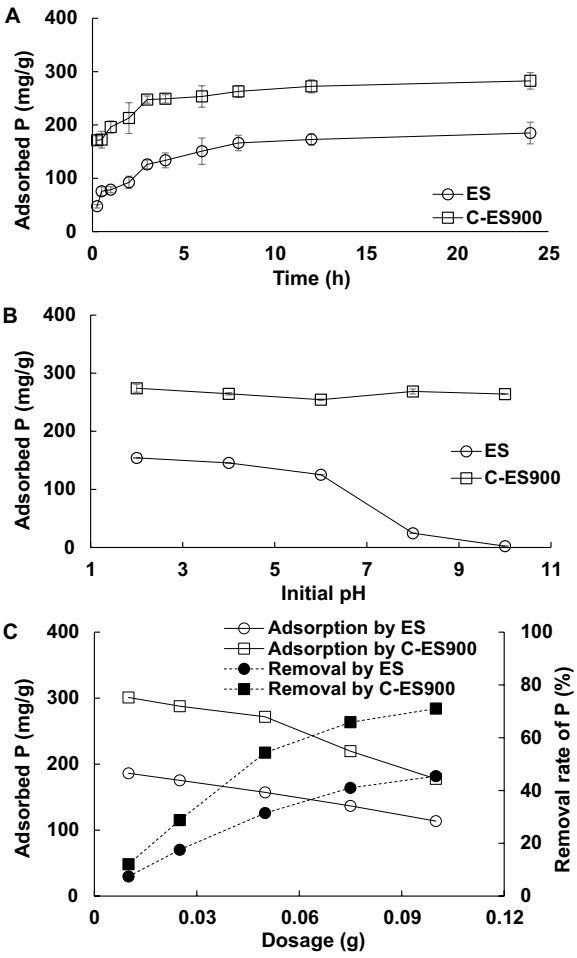

Fig. 3 Effects of contact time **A**, initial pH **B** and dosage **C** on phosphate adsorption by ES and C-ES900

Initial pH and adsorbent dosage

To evaluate the effect of pH on the phosphate sorption by ES and C-ES900, the pH of the aqueous phosphate solution was adjusted in the range of 2–10, and the results are shown in Fig. 3B. At pH 2, 4, 6, 8, and 10, the amount of phosphate adsorbed by ES was 154.3, 145.6, 125.3, 24.6, and 2.4 mg/g, respectively, indicating a relatively high sorption in an acidic solution. In general, the pH has a significant effect on the surface charge of the adsorbent and the chemical species of the contaminant. Phosphate exists mostly as $H_2PO_4^-$ at pH 3–7 [13] and is precipitated by the dissolved Ca^{2+} from the ESs. However, at a pH of 7 or higher, the surface charge of ESs is anionic, which causes a decrease in their sorption efficiency owing to the electrical repulsive force with the negatively charged phosphate. Similar results were also observed for calcite and crawfish shells, which are composed primarily of $CaCO_3$ [21, 31]. However, the amount of phosphate adsorbed by C-ES900 was in the range of 254.4–274.1 mg/g regardless of the initial pH. The final pH values of the solution after the sorption of phosphate by ES and C-ES900 were in the ranges of 7.5–8.1 and 8.8–10.2, respectively (data not shown), although there was a slight difference depending on the initial pH. Blanco et al. [32] reported that the removal of phosphate by the calcium-rich adsorbent was influenced by the ion-exchange mechanism and precipitation at pH < 8.5, whereas it was predominantly influenced by precipitation at pH > 8.5. Our results suggested that phosphate sorption by ES could be affected by ion exchange and partial precipitation, whereas with C-ES900, it may be predominantly affected by precipitation reaction.

Figure 3C shows the phosphate-sorption characteristics according to the doses of ES and C-ES900. In both ES and C-ES900, the phosphate removal efficiency increased as the dose increased, while the phosphate removal amount per unit gradually decreased. Similar results have been observed for calcium-rich adsorbents (concrete, fly ash, and biochar) in other studies [13, 33, 34]. When the dose of the adsorbent is increased, factors such as the

pH, solubility, and collision frequency in the sorption environment change, which has a decisive effect on the sorption amount. Mitrogiannis et al. [35] reported that as the ES dose increased, the amount of adsorbed pollutants decreased because of the formation of aggregates between the ES particles.

Co-existing anions

Domestic sewage and rivers contain a variety of anions, in addition to phosphate, such as Cl^-, NO_3^-, SO_4^{2-} and HCO_3^-. These anions are known to decrease the performance of the adsorbent, because they can increase the repulsive force for the active sites on the adsorbent surface or compete with phosphate. Therefore, the effect of various anions on the phosphate sorption characteristics of ES and C-ES900 was investigated, and the results are shown in Additional file 1: Fig. S2A. The amounts of phosphate adsorbed by ES in a phosphate solution with Cl^-, NO_3^- and SO_4^{2-} were 158.3, 157.5, and 145.3 mg/g, respectively, showing no significant difference compared with that in a solution with only phosphate (167.8 mg/g). In contrast, when phosphate and HCO_3^- coexisted, the amount of phosphate adsorbed by ES was 51.3 mg/g, which was significantly reduced compared with the phosphate-only solution. The amounts of phosphate adsorbed by C-ES900 were 228.42, 229.65, 224.07, and 164.0 mg/g in the presence of Cl^-, NO_3^-, SO_4^{2-}, and HCO_3^- together with phosphate, respectively. The amount of phosphate adsorbed by C-ES900 decreased rapidly in the presence of phosphate and HCO_3^-, similar to that with ES. Saadat et al. [36] reported that chloride and nitrate did not effectively compete with phosphate at the active site, because they were bound to the outer sphere of the adsorbent to form a complex, whereas phosphate was adsorbed through the inner sphere. Liu et al. [18] reported that in an aqueous solution, HCO_3^- binds to Ca^{2+} and is converted to an insoluble form, which is attached to the adsorbent surface and closes the active site where phosphorus would easily adsorb.

Salt concentration

The recent rise in sea level due to climate change can increase the salt concentration in nearby rivers. In particular, the presence of salt in an aqueous solution reduces the sorption capacity for specific pollutants through interactions with the adsorbent [37, 38]. The amount of phosphate adsorbed by ES was maintained at 121–134 mg/g until the salt concentration was 1%; however, at salt concentrations of 2% and 3%, the amount decreased to 74.1 and 65.9 mg/g, respectively (Additional file 1: Fig. S2B). Because the sorption of phosphate by the adsorbent is a surface phenomenon in which phosphate ions adhere to the adsorbent surface, the decrease in sorption capacity is related to the formation of a salt-based surface complex [39]. During the sorption process, the phosphate and adsorbent can form an inner-sphere complex, but when water molecules exist between the phosphate and adsorbent surface, an outer-sphere complex can also be formed. However, it is considered that the amount of phosphate adsorbed by ES decreases due to competition between phosphate ions and salt ions on the surface of the adsorbent at high salt concentrations. In contrast, the C-ES900 maintained a high sorption capacity even at a salt concentration of 3%. As mentioned above, because the sorption of phosphate by C-ES900 is predominantly influenced by precipitation rather than sorption on the surface, salt ions do not interfere.

Sorption mechanisms

To determine whether the phosphate-sorption process of calcium-rich ES and C-ES900 was sorption or precipitation, the content of Ca^{2+} ions eluted from each adsorbent before and after phosphate sorption was a critical factor. Therefore, the Ca^{2+} ion content eluted from ES and C-ES900 before phosphate sorption was investigated, and the results are shown in Fig. 4. The Ca^{2+} ion contents eluted from ES and C-ES900 were 4.2 and 48.9 mg/g before phosphate sorption and 2.7 and 0.1 mg/g after phosphate sorption, respectively. Park et al. [13] and Paradelo et al. [40] reported that when the phosphate-sorption properties were evaluated using calcium-rich fly ash, an excess of Ca^{2+} ions eluted from the fly ash and mussel shells before phosphate sorption and decreased rapidly after phosphate sorption. As can be seen from the results, the sorption of phosphate by C-ES900 was achieved by the precipitation of Ca^{2+} ions and phosphate ions released from the C-ES900 (Fig. 4).

SEM–EDS was performed to observe the changes in the surface structure and elemental distribution of ES

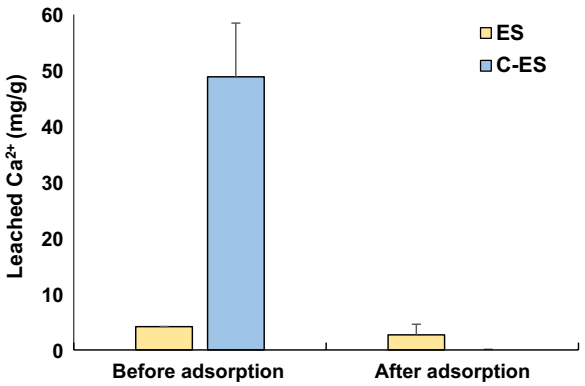

Fig. 4 Release characteristics of phosphate in ES and C-ES900 before and after phosphate adsorption

and C-ES900 before and after phosphate sorption, and the results are shown in Fig. 5. ES had a relatively smooth surface before the calcination process, whereas the surface of C-ES900 was exceptionally rough and had irregular crystalline structures. This is because the $CaCO_3$ was converted into CaO during the calcination process. In both the ES and C-ES900, a porous structure could not be observed after phosphate sorption, and more specific crystalline structures appeared than what were present before phosphate sorption. As a result of measuring the EDS, the surfaces of the ES and C-ES900 before phosphate sorption were mostly composed of C, O and Ca, whereas the presence of P was clearly observed after phosphate sorption, indicating that phosphate was successfully adsorbed onto the surfaces of ES and C-ES900.

The crystalline structures of ES and C-ES900 before and after phosphate sorption were analyzed using XRD, and the results are shown in Fig. 6. Several peaks appeared at 2θ values of 23.09°, 29.43°, 35.98°, 39.47°, 43.19°, 47.54°, 48.53°, and 57.56° in the ES, all of which are typical of $CaCO_3$ [41]. In contrast, for C-ES900, various peaks were observed at 2θ values of 17.94°, 28.57°, 34.08°, 47.13°, and 50.75°, which are mostly CaO-related [42]. These results showed that the thermal decomposition of ES composed of $CaCO_3$ led to the formation of CaO. After the sorption of phosphate, the intensity of the peaks related to $CaCO_3$ was weakened in the ES, and new peaks appeared at 20.95°, 30.55°, and 31.67° (2θ), which correspond to dicalcium phosphate dihydrate ($CaHPO_4$), β-TCP (tricalcium phosphate, $Ca_3(PO_4)_2$), and HAp(hydroxyapatite, $Ca_{10}(PO_4)_6(OH)_2$), respectively [43]. For C-ES900, new peaks were observed at 2θ values of 25.80°, 31.81°, and 50.19° after phosphate sorption, which are mostly related to HAp [44]. These results further prove that phosphate removal by ES and C-ES900 occurs via different mechanisms, as mentioned above.

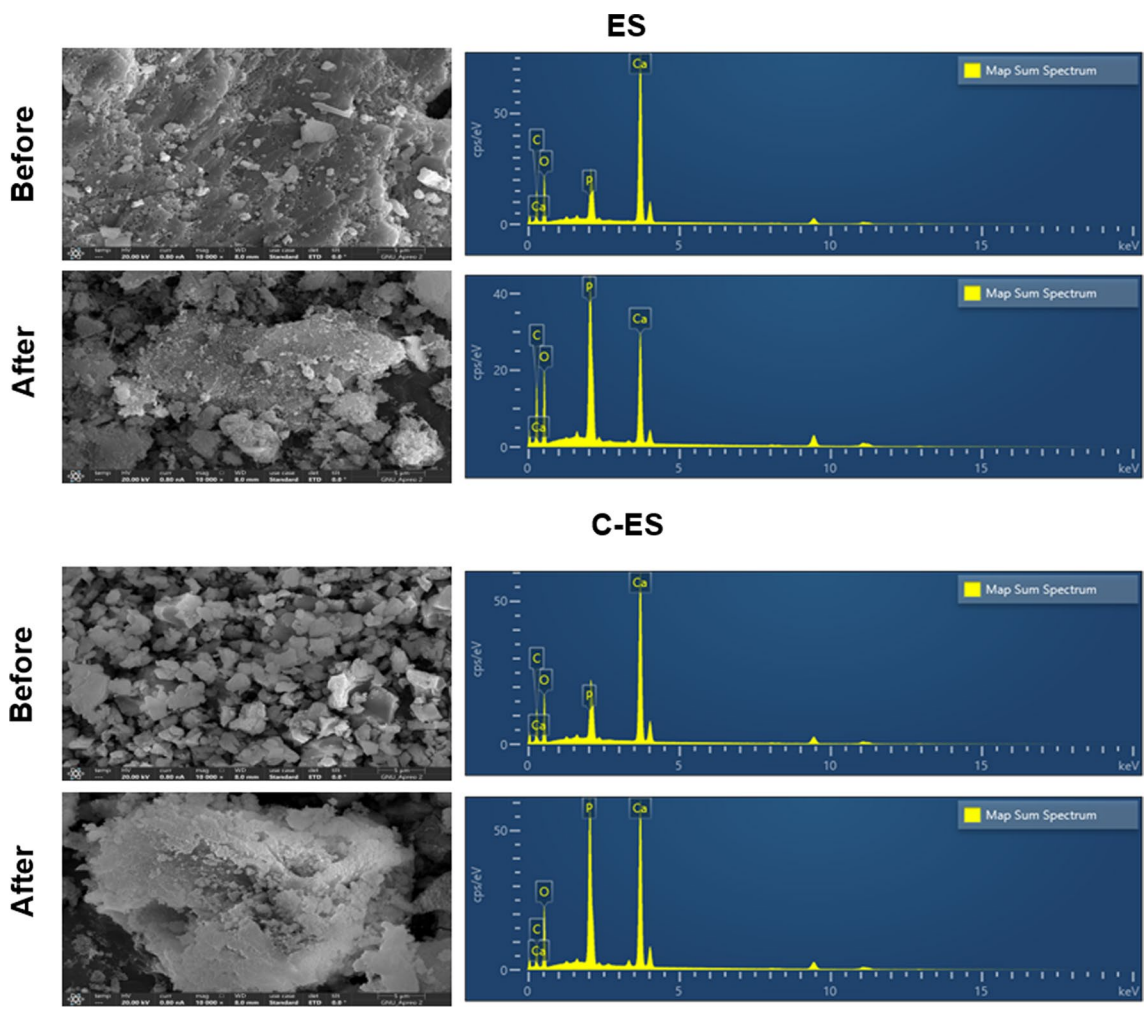

Fig. 5 Surface characteristics and element composition of ES and C-ES900 before and after phosphate adsorption

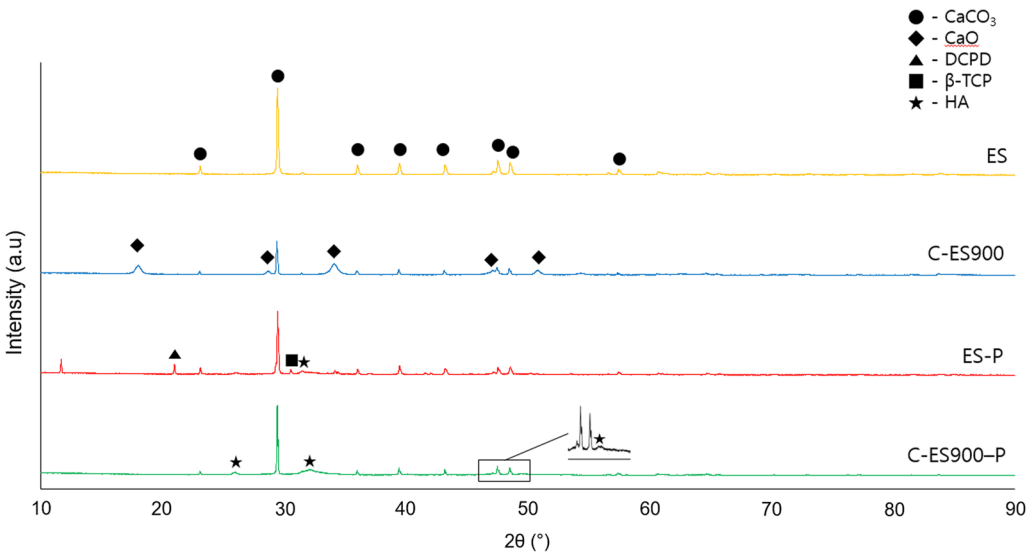

Fig. 6 Changes of crystalline structure in ES and C-ES900 before and after phosphate adsorption

As a result, C-ES900 manufactured through the ES calcination process can be used as an effective adsorbent to remove high concentrations of phosphate under a wide range of environmental conditions. In addition, the calcination of ESs to produce an adsorbent for water treatment will contribute to waste reduction and recycling.

Supplementary Information

The online version contains supplementary material available at https://doi.org/10.1186/s13765-022-00744-4.

Additional file 1. Table S1. Equations, plots, and constants for adsorption isotherm models. **Figure. S1.** Amounts of phosphate adsorbed by ES and C-ESs derived from different calcination temperature. **Figure. S2.** Effects of co-existing anions (A) and salt concentration (B) on phosphate adsorption by ES and C-ES900

Acknowledgements
This work was supported, in part, by the Green Fusion Technology Program funded by Ministry of Environment, by the National Research Foundation of Korea (NRF) grant funded by the Korea government(MSIT) [NRF-2022R1C1C1007804], and by the Korea Institute of Planning and Evaluation for Technology in Food, Agriculture and Forestry (IPET) through Livestock Industrialization Technology Development Program (121034-03) and Technology Commercialization Support Program (821007-03), funded by Ministry of Agriculture, Food and Rural Affairs (MAFRA).

Author contributions
J-HP, A-YC, S-HK and D-CS designed and conducted the experiment as well as wrote the manuscript. S-LL, J-HL and J-SR conducted characteristic analysis and interpretation of eggshell and Calcined-eggshells derived from different temperature used. All authors read and approved the final manuscript.

Funding
Not applicable.

Availability of data and materials
All data is available in the main text.

Declarations

Competing interests
The authors declare that they have no competing interests.

Author details
[1]Department of Life Resources Industry, Dong-A University, Busan 49315, South Korea. [2]Division of Applied Life Science (BK21) and Institute of Agriculture and Life Science, Gyeongsang National University, Jinju 52828, South Korea. [3]Soil and Fertilizer Management Division, National Institute of Agricultural Science, Rural Development Administration, Wanju 55365, South Korea.

Received: 17 August 2022 Accepted: 30 October 2022
Published online: 15 November 2022

References

1. Li B, Dong SL, Huang YF, Li P, Yu W, Wang GQ, Young B (2021) Toward a decision support framework for sustainable phosphorus management: a case study of China. J Clean Prod 279:123441
2. Awual MR (2019) Efficient phosphate removal from water for controlling eutrophication using novel composite adsorbent. J Clean Prod 228:1311–1319
3. Xia Y, Zhang M, Tsang DCW, Geng N, Lu D, Zhu L, Igalavithana AD, Dissanayake PD, Rinklebe J, Yang X, Ok YS (2020) Recent advances in control technologies for non-point source pollution with nitrogen and phosphorus from agricultural runoff: current practices and future prospects. Appl Biol Chem 63:8
4. Bektaş N, Akbulut H, Inan H, Dimoglo A (2004) Removal of phosphate from aqueous solutions by electro-coagulation. J Hazard Mater 106:101–105
5. Li S, Lin Z, Liu M, Jiang F, Chen J, Yang X, Wang S (2020) Effect of ferric chloride on phosphorus immobilization and speciation in Dianchi Lake sediments. Ecotoxicol Environ Safe 197:110637
6. Yang Q, Wang X, Luo W, Sun J, Xu Q, Chen F, Zhao J, Wang S, Yao F, Wang D, Li X, Zeng G (2018) Effectiveness and mechanisms of phosphate

adsorption on iron-modified biochar derived from waste activated sludge. Bioresour Technol 247:537–544
7. Peng H, Guo J (2020) Removal of chromium from wastewater by membrane filtration, chemical precipitation, ion exchange, adsorption electrocoagulation, electrochemical reduction, electrodialysis, electrodeionization, photocatalysis and nanotechnology: a review. Environ Chem Lett 18:2055–2068
8. Arslanoğlu H (2021) Production of low-cost adsorption with small particle size from calcium carbonate rich residue carbonatation cake and their high performance phosphate adsorption applications. J Mater Res Technol 11:428–447
9. Lee SL, Park JH, Kim SH, Kang SW, Cho JS, Jeon JR, Lee YB, Seo DC (2019) Sorption behavior of malachite green onto pristine lignin to evaluate the possibility as a dye adsorbent by lignin. Appl Biol Chem 62:37
10. Zhu F, Zheng YM, Zhang BG, Dai YR (2021) A critical review on the electrospun nanofibrous membranes for the adsorption of heavy metals in water treatment. J Hazard Mater 401:123608
11. Deng Y, Li M, Zhang Z, Liu Q, Jiang K, Tian J, Zhang Y, Ni F (2021) Comparative study on characteristics and mechanism of phosphate adsorption on Mg/Al modified biochar. J Environ Chem Eng 9:105079
12. Huo J, Min X, Wang Y (2021) Zirconium-modified natural clays for phosphate removal: effect of clay minerals. Environ Res 194:110685
13. Park JH, Hwang SW, Lee SL, Lee JH, Seo DC (2021) Sorption behavior of phosphate by fly ash discharged from biomass thermal power plant. Appl Biol Chem 64:43
14. Li W, Yu Q, Gu K, Sun Y, Wang Y, Zhang P, Zheng Z, Guo Y, Xin M, Bian R (2022) Stability evaluation of potentially toxic elements in MSWI fly ash during carbonation in view of two leaching scenarios. Sci Total Environ 803:150135
15. Lee JI, Oh JS, Yoo SC, Cho EH, Lee CG, Park SJ (2022) Removal of phosphorus from water using calcium-rich organic waste and its potential as a fertilizer for rice growth. J Environ Chem Eng 10:107367
16. Liu M, Li R, Wang J, Liu X, Li S, Shen W (2022) Recovery of phosphate from aqueous solution by dewatered dry sludge biochar and its feasibility in fertilizer use. Sci Total Environ 814:152752
17. Doustkhah E, Zare RN, Yamauchi Y, Taheri-Kafrani A, Mohtasham H, Esmat M, Ide Y, Fukata N, Rostamnia S, Sadeghi MH, Assadi MHN (2019) Template-oriented synthesis of hydroxyapatite nanoplates for 3D bone printing. J Mater Chem B 7:7228–7234
18. Liu X, Shen F, Qi X (2019) Adsorption recovery of phosphate from aqueous solution by CaO-biochar composites prepared from eggshell and rice straw. Sci Total Environ 666:694–702
19. Santos AF, Arim AL, Lopes DV, Gando-Ferreira LM, Quina MJ (2019) Recovery of phosphate from aqueous solutions using calcined eggshell as an eco-friendly adsorbent. J Environ Manage 238:451–459
20. Lee JI, Kim JM, Yoo SC, Jho EH, Lee CG, Park SJ (2022) Restoring phosphorus from water to soil: Using calcined eggshell for P adsorption and subsequent application of the adsorbent as a P fertilizer. Chemosphere 287:132267
21. Köse TE, Kıvanç B (2011) Adsorption of phosphate from aqueous solutions using calcined waste eggshell. J Chem Eng 178:34–39
22. Park JH, Wang JJ, Xiao R, Zhou B, Delaune RD, Seo DC (2018) Effect of pyrolysis temperature on phosphate adsorption characteristics and mechanisms of crawfish char. J Colloid Interf Sci 525:143–151
23. Choi D, Nam IH, Park YK, Ok YS, Lee J, Kwon EE (2019) Catalytic pyrolysis of brown algae using carbon dioxide and oyster shell. J CO2 Util 34:668–675
24. Ahmad R, Rohim R, Ibrahim N (2015) Properties of waste eggshell as calcium oxide catalyst. Appl Mech Mater 754–755:171–175
25. Bekiaris G, Peltre C, Jensen LS, Bruun S (2016) Using FTIR-photoacoustic spectroscopy for phosphorus speciation analysis of biochars. Spectrochim Acta A Mol Biomol Spectrosc 168:29–36
26. Chen P, Wang Y, He S, Wang P, Xu Y, Zhang L (2020) Green synthesis of spherical calcium hydroxide nanoparticles in the presence of tannic acid. Adv Mater Sci Eng 2020:9501897
27. Torit J, Phihusut D (2018) Phosphorus removal from wastewater using eggshell ash. Environ Sci Pollut Res 26:34101–34109
28. Panagiotou E, Kafa N, Koutsokeras L, Kouis P, Nikolaou P, Constantinides G, Vyrides I (2018) Turning calcined waste egg shells and wastewater to Brushite: Phosphorus adsorption from aqua media and anaerobic sludge leach water. J Clean Prod 178:419–428
29. Mezenner NY, Bensmaili A (2009) Kinetics and thermodynamic study of phosphate adsorption on iron hydroxide-eggshell waste. Chem Eng J 147:87–96
30. Guo Z, Li J, Guo Z, Guo Q, Zhu B (2017) Phosphorus removal from aqueous solution in parent and aluminum-modified eggshells: thermodynamics and kinetics, adsorption mechanism, and diffusion process. Environ Sci Pollut Res 24:14525–14536
31. Karageorgiou K, Paschalis M, Anastassakis GN (2007) Removal of phosphate species from solution by adsorption onto calcite used as natural adsorbent. J Hazard Mater 139:447–452
32. Blanco I, Molle P, de Miera LES, Ansola G (2016) Basic oxygen furnace steel slag aggregates for phosphorus treatment. Evaluation of its potential use as a substrate in constructed wetlands. Water Res 89:355–365
33. dos Reis GS, Thue PS, Cazacliu BG, Lima EC, Sampaio CH, Quattrone M, Ovsyannikova E, Kruse A, Dotto GL (2020) Effect of concrete carbonation on phosphate removal through adsorption process and its potential application as fertilizer. J Clean Prod 256:120416
34. Wang Z, Miao R, Ning P, He L, Guan Q (2021) From wastes to functions: A paper mill sludge-based calcium-containing porous biochar adsorbent for phosphorus removal. J Colloid Inter Sci 593:434–446
35. Mitrogiannis D, Psychoyou M, Baziotis I, Inglezakis VJ, Koukouzas N, Tsoukalas N, Palles D, Kamitsos E, Oikonomou G, Markou G (2017) Removal of phosphate from aqueous solutions by adsorption onto $Ca(OH)_2$ treated natural clinoptilolite. Chem Eng J 320:510–522
36. Saadat S, Raei E, Talebbeydokhti N (2018) Enhanced removal of phosphate from aqueous solutions using a modified sludge derived biochar: Comparative study of various modifying cations and RSM based optimization of pyrolysis parameters. J Environ Manage 225:75–83
37. Luengo CV, Volpe MA, Avena MJ (2017) High sorption of phosphate on Mg-Al layered double hydroxides: Kinetic and equilibrium. J Environ Chem Eng 5:4656–4662
38. Zhang H, Elskens M, Chen G, Chou L (2019) Phosphate adsorption on hydrous ferric oxide (HFO) at different salinities and pHs. Chemospehre 225:352–359
39. Zhi Y, Zhang C, Hjorth R, Baun A, Duckworth OW, Call DF, Knappe DRU, Jones JL, Grieger K (2020) Emerging lanthanum (III)-containing materials for phosphate removal from water: A review towards future developments. Environ Int 145:106115
40. Paradelo R, Conde-Cid M, Cutillas-Barreiro L, Arias-Estévez M, Nóvoa-Muñoz JC, Álvarez-Rodríguez E, Fernández-Sanjurjo MJ, Núñez-Delgado A (2016) Phosphorus removal from wastewater using mussel shell: Investigation on retention mechanisms. Eco Eng 97:558–566
41. Patowary M, Pathak K, Ananthakrishnan R (2015) A facile preparation of superhydrophobic and oleophilic precipitated calcium carbonate sorbent powder for oil spill clean-ups from water and land surfaces. RSC Adv 5:79852–79859
42. Fayyazi E, Ghobadian B, van de Bovenkamp HH, Najafi G, Hosseinzadehsamani B, Heeres HJ, Yue J (2018) Optimization of biodiesel production over chicken eggshell-derived CaO catalyst in a continuous centrifugal contactor separator. Ind Eng Chem Res 57:12742–12755
43. Laonapakul T, Sutthi R, Chaikool P, Talangkun S, Boonma A, Chindaprasirt P (2021) Calcium phosphate powders synthesized from $CaCO_3$ and CaO of natural origin using mechanical activation in different media combined with solid-state interaction. Mater Sci Eng C 118:111333
44. Han M, Kong L, Hu X, Chen D, Xiong X, Zhang H, Su M, Diao Z, Ruan Y (2018) Phase migration and transformation of uranium in mineralized immobilization by wasted bio-hydroxyapatite. J Clean Prod 197:886–894

Publisher's Note